Appl Nanosci (2017) 7:117–124
DOI 10.1007/s13204-017-0555-1

ORIGINAL ARTICLE

Synthesis of ammonium and sulfate ion-functionalized titanium dioxide for photocatalytic applications

J. L. Cheng[1] · J. Y. Mi[1] · H. Miao[1] · B. S. A. Sharifah Fatanah[1] · S. F. Wong[1] · B. K. Tay[1]

Received: 23 January 2017 / Accepted: 6 March 2017 / Published online: 14 March 2017

Abstract Due to high band gap energy the optimum photocatalytic activities can only be achieved under UV light, thus limiting the practical application of TiO_2. In this study, a method combining NH_4^+/SO_4^{2-}-functionalization technique and post-treatment was developed and successfully applied to synthesize photoactive TiO_2 samples which showed higher photocatalytic activity than the commercial P25 TiO_2 under visible light radiation. The results also showed that the addition of $(NH_4)_2SO_4$ surface functionalization on TiO_2 increased the photocatalytic activity, which could be due to the combined effect of crystallinity and band gap energies. Moreover, the results showed that calcination temperature was inversely proportional to photocatalytic activity. The degradation efficiency for methylene blue under visible light was improved by ~2 times from 10.7% for P25 nano Degussa TiO_2 to 20.2% for the synthesized sample. The band gap energies were also reduced from 3.7 to 3.4 eV (under UV–Vis direct transition mode) indicating a red shift towards higher wavelength.

✉ J. L. Cheng
jlcheng@tp.edu.sg

J. Y. Mi
1405839J@student.tp.edu.sg

H. Miao
miaoh@TP.EDU.SG

B. S. A. Sharifah Fatanah
sfatanah@TP.EDU.SG

S. F. Wong
drsfwong@tp.edu.sg

B. K. Tay
bktay@tp.edu.sg

[1] School of Applied Science, Temasek Polytechnic, 21 Tampines Avenue 1, Singapore 529757, Singapore

Keywords X-ray diffraction · Nanostructured materials · Ceramics · Powder metallurgy · Grain growth · Grain refinement

Introduction

In recent times, the use of TiO_2 for photocatalytic purposes has attracted much attention. This is mainly due to TiO_2 having many advantages over other photocatalysts. It has been proven to be nontoxic, biologically inert, physically and chemically stable against corrosion (Yu et al. 2006). Nevertheless, some characters limit the practical application of TiO_2. For example, the high band gap energy of TiO_2 causes that the optimum photocatalytic activities to be achieved only with the presence of ultraviolet (UV) light. Hence, the usage of solar energy is insufficient for TiO_2 as solar light only contains 4 or 5% of UV radiation, whereas visible light radiation contributes 45% of solar energy (Yu et al. 2006; Dong et al. 2015).

Previous studies had developed various functionalization methods by doping metal elements on TiO_2 to lower the band gap energy, subsequently achieving higher efficiency of absorbing visible light. The common metal elements used are, for example, silver, nickel, copper, iron, manganese, etc. (Dong et al. 2015; Garza-Arévalo et al. 2016). However, metal doping is relatively expensive in its application, whereas non-metal functionalization is comparatively more economical and results in decreased band gap energy of TiO_2 (Yu et al. 2006; Sajid and Moo 2016; Zhang et al. 2015; Govindan et al. 2013). Moreover, a study had shown that single anatase phase, which is the favorable phase to carry out photocatalytic activity (Dong et al. 2015) was observed in NH_4^+/SO_4^{2-}-functionalized

TiO_2 sample synthesized via hydrolysis of $TiOSO_4$ with the addition of $(NH_4)_2SO_4$ (Toibah et al. 2015).

In addition, small particle size, increased crystallinity and high porosity had been reported in previous studies to further improve photocatalytic performance (Tian et al. 2009; Elgh et al. 2014; Ren et al. 2014). Post-treatment methods using hydrothermal treatment and calcination are often used to improve these properties in TiO_2. Hydrothermal treatment had been proven to be able to yield smaller and more evenly distributed TiO_2 particles (Montazeri-Pour et al. 2013). Moreover, a previous study has also reported that, after hydrothermal treatment, NH_4^+/SO_4^{2-}-functionalized TiO_2 samples showed a special orientation of crystallites, which resulted in decent increase in crystallinity (Salim et al. 2011). Calcination, in addition, is a rapid thermal treatment method to increase the crystallinity of TiO_2 but at too high calcination temperature will result in the formation of unfavorable rutile phase of TiO_2 and largely reduce the particle surface area due to drastically increased crystalline size, thus hindering the photocatalytic performance (Garza-Arévalo et al. 2016). Hence, a range of calcination temperatures was studied to determine the optimum calcination condition in terms of photocatalytic performance (Garza-Arévalo et al. 2016).

In view of the various findings, this study describes a combination of NH_4^+/SO_4^{2-} functionalization, hydrothermal treatment and calcination to yield TiO_2 with photocatalytic performance under visible light and to determine the effect of the addition of $(NH_4)_2SO_4$ and the effect of different calcination temperatures on the photocatalytic performance of synthesized TiO_2 in comparison to the commonly used commercial Degussa P25 TiO_2.

Materials and methods

Precursors used to synthesize functionalized TiO_2 were titanium (IV) oxide sulfate sulfuric acid hydrate ($TiOSO_4.xH_2O + H_2SO_4$) and ammonium sulfate ($(NH_4)_2SO_4$) purchased from Alfa Aesar and VWR chemicals, respectively. The photocatalytic performance and its related properties of all synthesized sample were compared with Degussa P25 titanium (IV) dioxide nanopowder (TiO_2) purchased from Aldrich. Methylene blue was purchased from J.T. Baker. All chemicals were in reagent grade. No further purification was performed for all chemicals. Deionized (DI) water was used throughout the experiment.

The synthesis of the functionalized TiO_2 was conducted through hydrolysis reaction of $TiOSO_4$ stated in Eq. (1).

$$TiOSO_4(s) + 2H_2O\,(aq) \rightarrow SO_4^{2-}(aq) + 2H^+(aq) + TiO(OH)_2(s) \quad (1)$$

Immediately after the $TiOSO_4$ was added into DI water, the required amount of $(NH_4)_2SO_4$ was slowly added to make up a certain mol% of $(NH_4)_2SO_4$ in the mixture. At this stage, NH_4^+ and SO_4^{2-} ions from $(NH_4)_2SO_2$ and SO_4^{2-} ions from $TiOSO_4$ are functionalized onto $TiO(OH)_2$ surface. The white mixture was heated up to 80 °C for 8 h. The subsequent drying of the precipitate allows the water content to be removed from $TiO(OH)_2$, hence resulting in crystalline TiO_2 as shown in Eq. (2).

$$TiO(OH)_2(\text{amorphous}) \rightarrow H_2O\,(g) + TiO_2(\text{crystalline}) \quad (2)$$

The resulted sample undergoes hydrothermal treatment with DI water at 150 °C for 5 h. The resulted sample was collected through centrifugation and dried at 60 °C for 12 h. The calcination temperature was varied at 500, 600 and 700 °C, respectively, for 1 h in a vacuum furnace to study the effects of calcination temperature. A summary of sample name and information is stated in Table 1.

The powders obtained were characterized using various techniques. A scanning electron microscope (SEM) (JEOL JSM-6360A) was used to analyze the size and morphology of the powders. The SEM is equipped with energy dispersive X-ray spectrometer (EDX) that allows elemental analysis. The X-ray diffraction patterns of the powders were obtained with a BRUKER ADVANCE X-ray powder diffractometer using a Cu target ($\lambda_{Cu\ K\alpha} = 1.5405$ Å). FTIR analysis was done using SHIMADZU IR Prestige-21 Fourier transform infrared spectrophotometer. The diffuse refractive spectra of all samples were obtained using SHIMADZU UV-2600 UV–Vis spectrophotometer with integrating sphere attachment.

Table 1 Summary of sample information

Sample name	Synthesis	Hydrothermal	Calcination
500-w	8 h hydrolysis with $(NH_4)_2SO_4$	150 °C for 5 h	500 °C for 1 h
600-w	8 h hydrolysis with $(NH_4)_2SO_4$	150 °C for 5 h	600 °C for 1 h
700-w	8 h hydrolysis with $(NH_4)_2SO_4$	150 °C for 5 h	700 °C for 1 h
Degussa P25 TiO_2 nanopowder	TiO_2 with average particle size of 21 nm		

Results and discussion

The FTIR spectra of the samples are shown in Fig. 1. The broad peaks ranging from 436 to 653 cm^{-1} were observed in all samples and assigned to the vibration of Ti–O and Ti–O–Ti group (Bezrodna et al. 2004). Errant peaks were observed around 2350 cm^{-1}, which were due to the interference of CO_2 in the atmosphere (Smith 2011). The graph showed successful functionalization of SO_4^{2-} ions in sample 500, 600, 700-w samples indicating peaks observed at 1135 and 1040 cm^{-1} due to the vibration of O=S=O and Ti–O–S which is consistent with the reported works, whereby the SO_4^{2-} groups functionalized via incorporation into the lattice structure of TiO_2 (Yang et al. 2012). Moreover, the FTIR spectra showed that as calcination temperature increased, the SO_4^{2-} peak intensity decreased. This implies that high calcination temperature favored the desorption of SO_4^{2-} from TiO_2 sample.

The peaks in the range of 3100–3750 cm^{-1} and around 1620 cm^{-1} were commonly reported in TiO_2 samples, which were assigned to the stretching vibration of TiO_2 surface hydroxyl groups and deformation vibration of adsorbed water molecules, respectively (Beranek and Kisch 2008). The stretching and deformation vibrations modes of NH_x groups also existed in these two regions, subsequently resulting in overlapped peaks with hydroxyl groups and water molecules (Beranek and Kisch 2008). SEM analysis and EDX mapping shown in Fig. 2 was done on sample 600-w with detection of nitrogen atoms with titanium and sulfur with particle size of ~2 to 3 μm. The EDX mappings indicate the presence of nitrogen and sulfur which are consistent with the FTIR results showing the successful functionalization of the synthesized powders. The larger particle size in sub-micron range for the synthesized powder indicates that in consideration of size effects, the photocatalytic performance of nano-P25 TiO_2 (average APS ~25 nm) are expected to perform better due increased surface area with a smaller particle size. However, other contributing factors such as phase purity (Dong et al. 2015), band gap energies and presence of surface groups (Salim et al. 2011) may be more dominant than size effects.

Figure 3 shows the XRD spectrums in all synthesized samples, whereas rutile phase appeared in commercial P25 TiO_2. The percentage of rutile phase calculated by TOPAS was 23.43% in P25 which is commonly found in nano-TiO_2. Characteristic anatase peaks were found in all synthesized samples with no rutile phase observed. For maximum photocatalytic organic degradation application in regards with TiO_2 crystalline phases, it will be preferred to remain in the anatase phase (Dong et al. 2015).

The anatase phase crystalline size of sample 500, 600, 700-w, and P25 were calculated to be 14.6, 23.0, 43.3, and 20.2 nm, respectively, using Debye–Scherer formula (Lebedeva et al. 2014):

$$D = \frac{k\lambda}{\beta \cos\theta}. \quad (3)$$

The peak width at half of the maximum peak intensity, β and incident angle value at the maximum peak, θ were

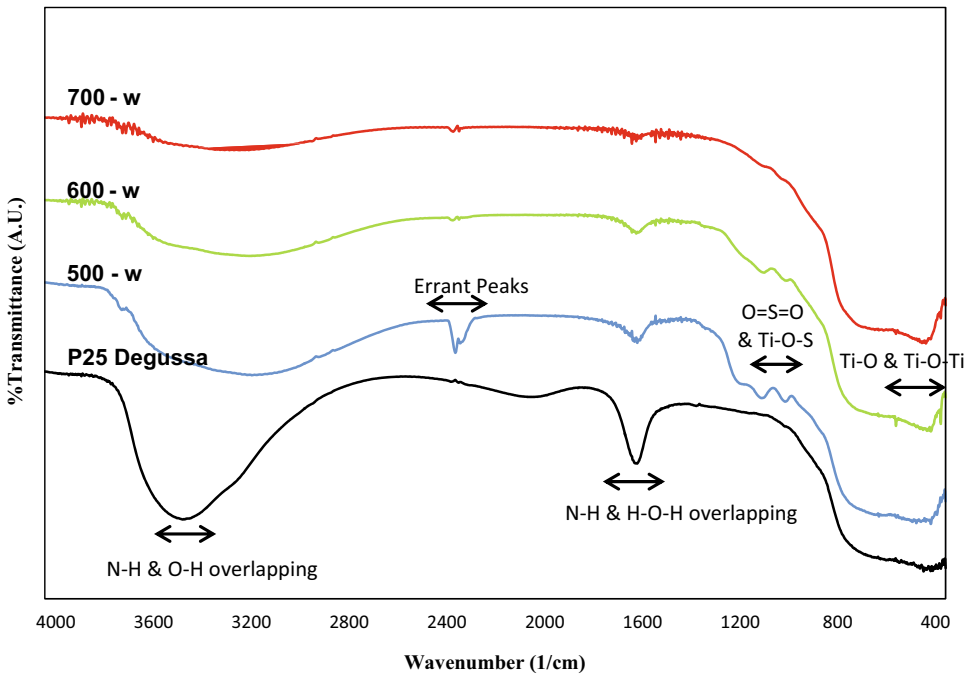

Fig. 1 FTIR analysis of synthesized samples

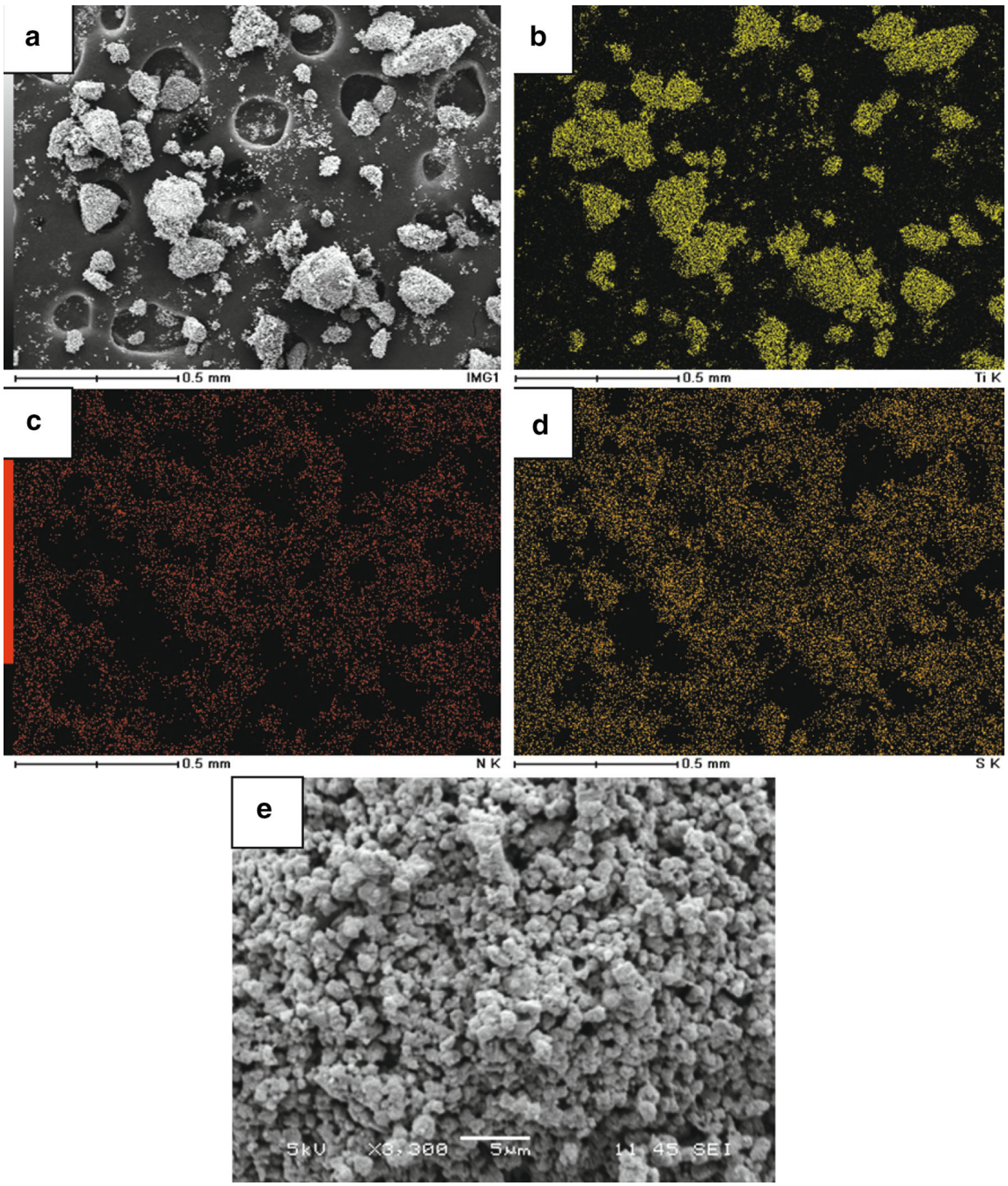

Fig. 2 **a** Elemental mapping of sample 600-w TiO_2 with **b** titanium in *yellow*, **c** nitrogen in *red*, **d** sulfur in *orange* and **e** magnified view showing particle size of ~2 to 3 µm

determined from the respective XRD graph with the dimensionless shape factor k of 0.89 at the wavelength of X-ray source λ (Cu K alpha) of 0.154050 nm.

The changes in crystalline size of synthesized samples were in line with the changes in peak sharpness and intensity, suggesting that variation of crystallinity of synthesized samples was mainly determined by the size of crystallites. An increasing trend of peak intensity and crystalline size was observed in sample 500, 600 and 700-w, suggesting that the increase in calcination temperature resulted in further growth of crystalline size, hence favoring the formation of TiO_2 with higher crystallinity. On the other hand, no rutile phase was observed in these samples, suggesting that the applied calcination temperature was not high enough to cause phase transformation (Fig. 4).

The resulted UV–Vis spectra were converted to $(h\nu\alpha)^{1/r}$ versus $h\nu$ graph. The value r was set at ½ for direct allowed

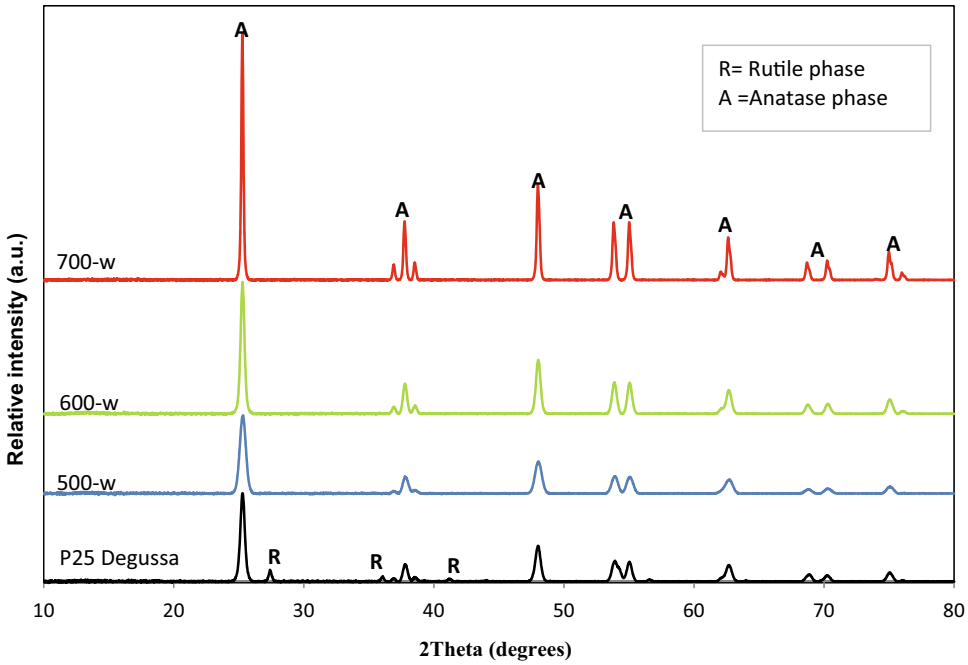

Fig. 3 X-ray diffraction patterns of different calcination-treated samples in comparison to Degussa P25 TiO_2 nanopowder

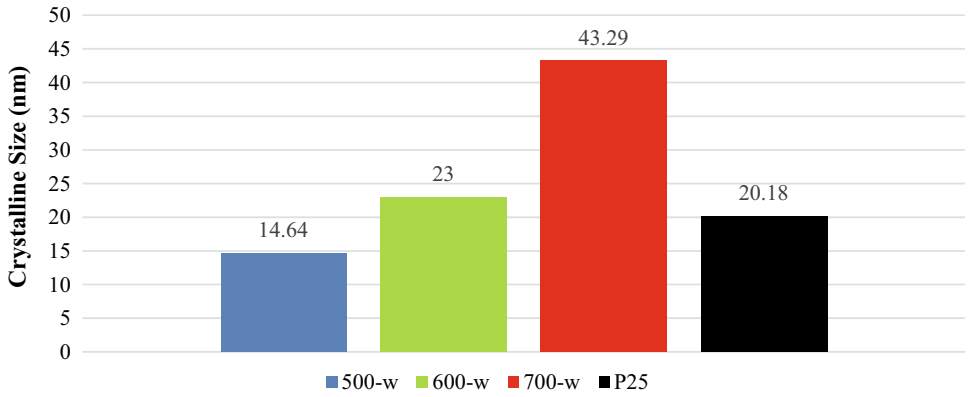

Fig. 4 Comparison of crystalline size value of sample 500, 600, 700-w, and P25

transition. hv was the product of h (Plank's constant) and v (frequency of vibration) and the relationship between hv and wavelength (λ) was $hv = 1239.7/\lambda$. Using the Kubelka–Munk function (Philips-Invernizzi 2001)

$$F(R) = \frac{(1-R)^2}{2R}, \tag{4}$$

the % reflectance (R) values were converted to quantity $F(R)$, which was proportional to absorption coefficient, α. In the actual experiment, α was substituted by $F(R)$. On the $(hv\alpha)^{1/r}$ versus hv curve, the line, which was tangent to the point of inflection, was drawn. The band gap energy (Eg) was obtained at the intersection point of tangent line and hv axis. The equation of tangent line was shown as Tauc's equation (Bhatt et al. 2011):

$$(hva)^{1/r} = A(hv - \mathrm{Eg}). \tag{5}$$

The results in Fig. 5 showed that the band gap value of 500, 600 and 700-w were very close to each other, suggesting that the changes in calcination temperature caused insignificant effect on the band gap energy of TiO_2. All synthesized samples showed lower band gap energy indicating red shifts towards the visible range as compared to P25.

To carry out photocatalytic test, 2 g of TiO_2 sample was mixed with 40 ml of 10 ppm methylene blue solution in 80 ml of beaker. The mixture was then stirred under dark environment for 1 h in order for the methylene blue and TiO_2 sample to reach adsorption–desorption equilibrium. Subsequently, the mixture was stirred under visible light radiation generated by domestic lamp for 5 h. 4 ml of mixture was extracted using CELLOTRON 10 ml disposable syringe at time = 0, 1, 2, 3, 4, 5 h. The extracted mixture was immediately filtered through PALL 0.2 μm

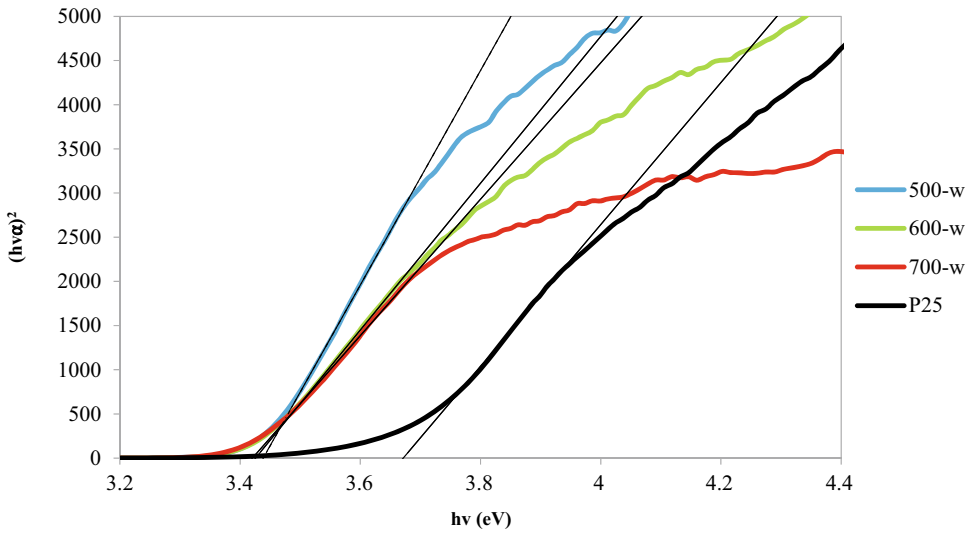

Fig. 5 Illustration of Tauc plot for sample 500, 600, 700-w and P25

syringe filter with PES membrane to obtain clear methylene blue solution. The absorbance of the solution was measured by SHIMADZU UV-1800 UV spectrophotometer and wavelength of radiation source was set at 664 nm. The obtained absorbance value was then used to draw % absorbance versus time graph and the degradation efficiency for the respective sample was calculated by the equation:

$$\%D = \frac{[\mathrm{Abs}]_{t=0} - [\mathrm{Abs}]_{t=5}}{[\mathrm{Abs}]_{t=0}} \times 100\%. \quad (6)$$

Figure 6 shows the methylene blue degradation results whereby all samples showed decreasing trends of methylene blue concentration and the difference became more distinct with time. Figure 7 shows the highest degradation efficiency of 20.2% in sample 500-w and P25 Degussa nanopowder having the lowest degradation efficiency of 10.7%.

All analysis was conducted using the UV–Vis spectrometer under the direct transition mode. The nano-P25 Degussa TiO_2 which corresponds to ~3.7 eV is in good

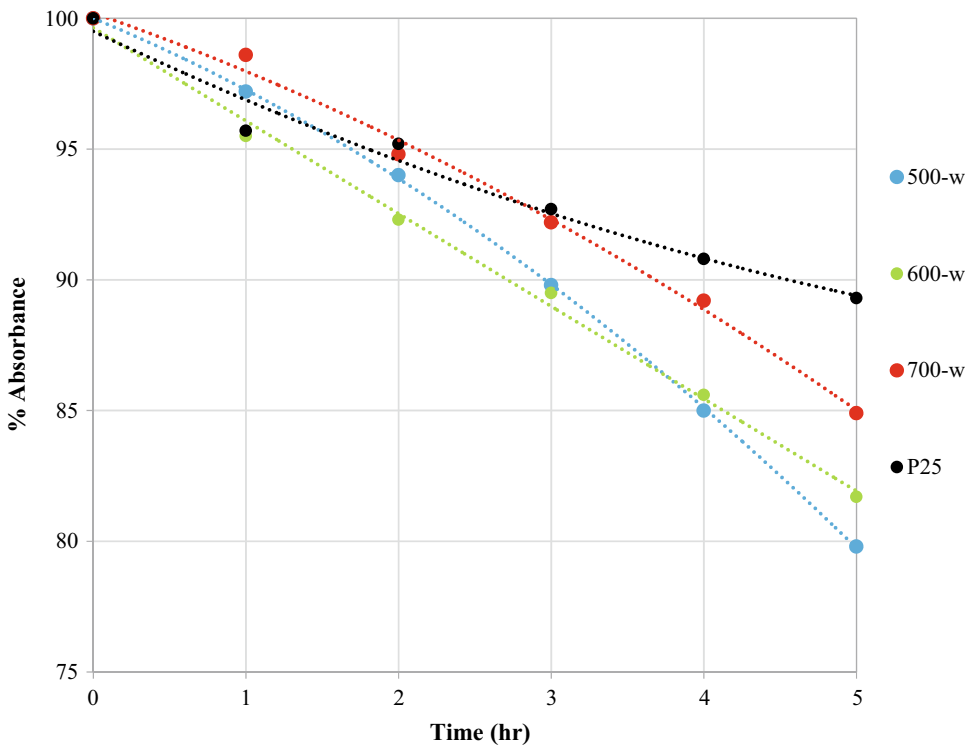

Fig. 6 Methylene blue degradation trend of sample 500, 600, 700-w, and P25

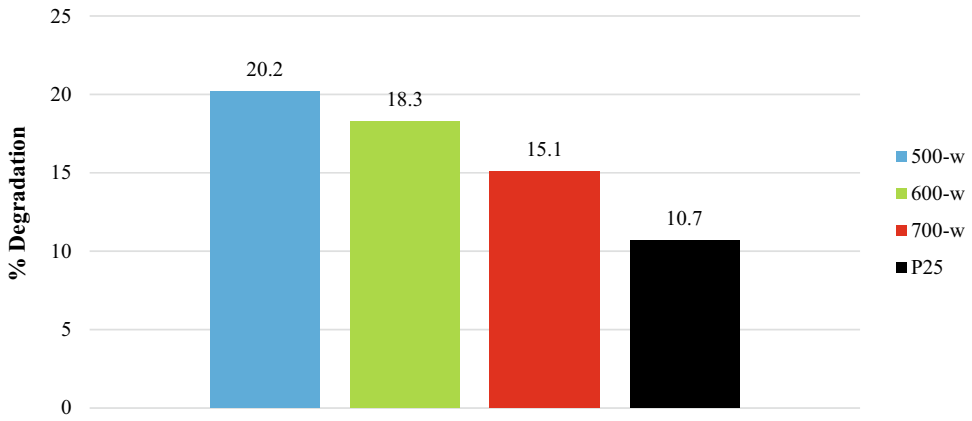

Fig. 7 Degradation efficiency of sample 500, 600, 700-w, and P25 in 5 h

agreement with previous research studies reported in literature (Sergio et al. 2010). As such, in relation to the measured nano-P25 TiO_2, all the functionalized samples showed a decrease in band gap values from 3.7 to ~3.4 eV indicating a red shift in wavelength. A combination of pure anatase phase shown in the XRD results, NH_4^+/SO_4^{2-} functionalization shown in FTIR/EDX and reduced band gap energies may be the dominant contributing factors in better photocatalytic activity shown by the synthesized powders compared to the smaller particle sized nano-TiO_2.

The reducing trend of degradation efficiency in sample 500, 600 and 700-w suggests that increase in calcination temperature could hinder photocatalytic performance. The trend could be explained by combined effect of the crystallinity and crystalline size. XRD spectra showed that crystallinity increased with calcination temperature and it is commonly accepted fact that high crystallinity is favored to carry out photocatalytic reaction, because it can resist the recombination of photo-generated holes and electrons back to ground state hence resulting in more radicals to degrade organics (Tian et al. 2009). Nevertheless, the growth of crystalline size due to high temperature also drastically reduced TiO_2 surface area, resulting in less contact with methylene blue molecules and lowering the photocatalytic activity (Yu et al. 2006; Garza-Arévalo et al. 2016). In this study, amongst these two factors, the effect of crystallinity could have been overwhelmed by the effect of crystalline size, hence resulting in an overall decreasing trend of performance as calcination temperature increased with the optimal calcination temperature found to be at 500 °C with the highest degradation efficiency.

Conclusions

In conclusion, NH_4^+/SO_4^{2-}-functionalized TiO_2 was successfully synthesized through hydrolysis reaction and post-treatments and all samples showed higher photocatalytic activity than Degussa P25 TiO_2 nanopowder under visible light. The sample calcined at 500 °C had the strongest photocatalytic activity which was 88.8% higher than nano-sized P25 TiO_2 due to its relatively smaller crystalline size, lower band gap energy and single anatase crystal phase. Furthermore, the results suggest that photocatalytic activity of functionalized TiO_2 was inversely proportional to calcination temperature. This is because the induced crystalline growth dominates the effect.

Acknowledgements The authors thank the Ministry of Education Translation and Innovation Fund (Singapore) (Grant Number: MOE2015-TIF-1-G-038) for funding and support given to this project.

References

Beranek R, Kisch H (2008) Tuning the optical and photoelectrochemical properties of surface-modified TiO_2. Photochem Photobiol Sci 7(1):40–48

Bezrodna T, Puchkovska G, Shymanovska V, Baran J, Ratajczak H (2004) IR-analysis of H-bonded H_2O on the pure TiO_2 surface. J Mol Struct 700(1–3):175–181

Bhatt R, Bhaumik I, Ganesamoorthy S, Karnal AK, Swami MK, Patel HS, Gupta PK (2011) Urbach tail and bandgap analysis in near stoichiometric $LiNbO_3$ crystals. Phys Status Solidi (a) 209(1):176–180

Dong H, Zeng G, Tang L, Fan C, Zhang C, He X, He Y (2015) An overview on limitations of TiO_2-based particles for photocatalytic degradation of organic pollutants and the corresponding counter measures. Water Res 79:128–146

Elgh B, Yuan N, Cho HS, Magerl D, Philipp M, Roth SV, Palmqvist AE (2014) Controlling morphology, mesoporosity, crystallinity, and photocatalytic activity of ordered mesoporous TiO_2 films prepared at low temperature. APL Mater 2(11):113313

Garza-Arévalo JI et al (2016) Fe doped TiO_2 photocatalyst for the removal of As(III) under visible radiation and its potential application on the treatment of As-contaminated groundwater. Mater Res Bull 73:145–152

Govindan K et al (2013) Photocatalytic degradation of pentachlorophenol in aqueous solution by visible light sensitive N F-codoped TiO_2 photocatalyst. Mater Res Bull 48:1913–1919

Lebedeva II, Sizeneva IP, Kisel'Kov DM, Val'Tsifer VA (2014) Study of the effect of ammonium sulfate additives on the structure and photocatalytic activity of titanium dioxide. Russ J Appl Chem 87(5):547–554

Montazeri-Pour M, Riahi-Noori N, Mehdikhani A (2013) Synthesis of single-phase anatase TiO_2 nanoparticles by hydrothermal treatment with application potential for photoanode electrodes of dye sensitized solar cells. J Ceram Process Res 14:595–600

Philips-Invernizzi B (2001) Bibliographical review for reflectance of diffusing media. Opt Eng 40(6):1082

Ren L, Li Y, Hou J, Zhao X, Pan C (2014) Preparation and enhanced photocatalytic activity of TiO_2 nanocrystals with internal pores [Abstract]. ACS Appl Mater Interfaces 6(3):1608–1615

Sajid AA, Moo HC (2016) Highly visible light responsive, narrow band gap TiO_2 nanoparticles modified by elemental red phosphorus for photocatalysis and photoelectrochemical applications. Nat Sci Rep 6:25405

Salim NT, Yamada M, Nakano H, Fukumoto M (2011) The synthesis of titanium dioxide (TiO_2) powder for cold spray process. IOP Conf Ser Mater Sci Eng 18(3):032019

Sergio V, Juan MM, Gloria R (2010) Study of the bandgap of synthesized titanium dioxide nanoparticles using the sol-gel method and a hydrothermal treatment. Open Mater Sci J 4:9–14

Smith BC (2011) Fundamentals of Fourier transform infrared spectroscopy, 2nd edn. CRC Press Taylor & Frances Group, Boca Raton, FL

Tian G, Fu H, Jing L, Tian C (2009) Synthesis and photocatalytic activity of stable nanocrystalline TiO_2 with high crystallinity and large surface area. J Hazard Mater 161(2–3):1122–1130

Toibah AR, Sato M, Yamada M, Fukumoto M (2015) Cold-sprayed TiO_2 coatings from nanostructured ceramic agglomerated powders. Mater Manuf Processes 31(11):1527–1534

Yang G, Yan Z, Xiao T (2012) Low-temperature solvothermal synthesis of visible-light-responsive S-doped TiO_2 nanocrystal. Appl Surf Sci 258(8):4016–4022

Yu J, Zhou M, Cheng B, Zhao X (2006) Preparation, characterization and photocatalytic activity of in situ N, S-codoped TiO_2 powders. J Mol Catal A Chem 246(1–2):176–184

Zhang J, Xu LJ, Zhu ZQ, Liu QJ (2015) Synthesis and properties of (Yb, N)-TiO_2 photocatalyst for degradation of methylene blue (MB) under visible light irradiation. Mater Res Bull 70:358–364